Theoretical investigation of the isomer shifts of the ^{119}Sn Mössbauer isotope

A. Svane* and E. Antoncik
Institute of Physics, University of Aarhus, 8000-Aarhus C, Denmark
(Received 30 May 1986)

We solve the electronic structure problem self-consistently for a series of crystalline solids, containing Sn as a component, with the use of the first-principles scalar-relativistic linear muffin-tin-orbital method in the local-density approximation. The crystals considered are the two allotropes α-Sn and β-Sn as well as the compounds SnO_2, $SnMg_2$, SnSb, and SnTe. The derived band structure is discussed and compared to previous calculations and experimental information. By extension of the radial integration of the Dirac equation to well within the nuclear regime, the valence-electron contribution to the charge density on the nuclear site is obtained. Excellent agreement is found when comparing with experimental isomer shifts. A value of $\Delta R/R=(1.34\pm0.07)\times10^{-4}$ for the relative change of the radius of the ^{119}Sn nucleus upon excitation is deduced. The observed trends in the isomer shifts are interpreted on the basis of the decomposition of the crystal wave function into angular momentum character.

I. INTRODUCTION

The isomer shift of the 23.875-keV resonance of the ^{119}Sn Mössbauer isotope has found wide application as a spectroscopic tool for investigating the electronic structure of solid-state systems.[1,2] For the basic research on the elemental semiconductors and semiconducting compounds the ^{119}Sn isotope has proven valuable as a probe to monitor the local chemical bond. Thus, when substitutionally implanted in the group-IV semiconductors[3] and III-V compounds,[4] the measured isomer shift reveals information on the electronic and vibrational properties of the host crystal.[5–8] For pure crystalline solids the Mössbauer isomer shift can also provide valuable information on the electronic structure, and the present work is aimed at the interpretation of isomer shifts in some compounds, in which Sn represents a component. The crystals studied are the two allotropes of tin, α-Sn, and β-Sn, as well as the largely covalent binaries of SnSb, SnTe, and $SnMg_2$ and the ionic rutile-structured SnO_2.

The isomer shift is related to the change in transition energy between two nuclear levels, which is caused by the electrostatic interaction of the nuclear charge distributions with the surrounding electron gas:[9]

$$\Delta_{IS}=\alpha(\rho_a(0)-\rho_s(0)) , \quad (1)$$

where Δ_{IS} is the resonant isomer-shift velocity, $\rho_a(0)$ and $\rho_s(0)$ are the electron densities on the nuclear site (the contact densities) in the absorber and source materials, respectively, and α is the nuclear calibration constant, which is often parametrized in terms of the relative change in nuclear radius between the two levels involved as $\alpha=\gamma\Delta R/R$, where γ is a numerical constant.[10]

The extraction of the optimum information about the solid state from isomer-shift measurements requires an accurate value of the calibration constant α to facilitate a conversion to density units. Being a purely nuclear factor, α could be determined from first-principles nuclear-physics models, but these have not yet reached a level of accuracy that suffices for the present purpose.[11] To keep the present calculations reasonably simple, we represent the nucleus by a uniformly charged sphere of radius $R=1.2A^{1/3}$ fm, where A is the atomic mass. The values of $\rho(0)$ in Eq. (1) have been obtained as mean values of the self-consistent electron densities in the nuclear volume. There is no doubt that the model of the nucleus adopted has some effect on the contact densities, but we are convinced that the model of the uniformly charged nucleus is superior to the point nucleus or to some other models containing several additional parameters not always known with the precision needed.[9]

The usual line of attack has until now been to compare the experimental values of Δ_{IS} in Eq. (1) with calculated or independently measured electron contact densities. The latter approach utilizes the internal conversion[12] of valence electrons in a solid, but only few such experiments have been reported.[13] This technique is, however, likely to become prominent in the future as experimental resolution improves.

By far the most common calibration procedure relies on calculated electron contact densities, and many approximations have been invoked to obtain this quantity. Generally, the use of atomic calculations is widespread, though recently also molecular and cluster calculations have been reported for some isotopes. To use atomic calculations for the calibration of Mössbauer isomer shifts one needs as extra input the assumption (or estimate) of some atomic configuration which can be taken as equivalent to the actual configuration in the solid. Furthermore, the Wigner-Seitz model[14] confines the atom to a finite sphere, which represents the amount of space allotted to the atom in the solid. This widely used model introduces as an extra parameter the radius of the sphere, and the proper value of this is not always easy to assess.[15]

Perhaps, the best attempts to calibrate Mössbauer isotopes along these lines have been those calculations which derive the equivalent atomic configuration—in terms of

the effective (fractional) occupancies Z_s and Z_p—from parametrized tight-binding calculations.[15,16] Subsequently, the electron contact density of the (confined) atom in the configuration $s^{Z_s}p^{Z_p}$ is calculated from a Dirac-Fock-Slater procedure. In this approach no presumptions on the electronic structure of the Mössbauer atom are used as input, but this information is rather derived from a solid-state scheme. However, still a number of adjustable parameters are present in such calculations, and they should only be regarded as a serious first step towards the proper incorporation of solid-state effects into the calculation of electron contact densities. In this work we calculate the electronic structure of the crystals that are of our concern, from a genuine first-principles solid-state calculational scheme, so that no estimates either on the appropriate radius or the effective configuration of the atom are required.

The linear muffin-tin-orbital (LMTO) method[17,18] has been adopted for this purpose. It has proven a fast and reliable method for determining the electronic structure of a variety of solid-state systems such as metals, semiconductors, and surfaces. In contrast to the tight-binding calculations mentioned above, this method allows us to iterate the crystal potential and charge distribution to self-consistency. The electron contact density is directly obtained by inspection, provided that the radial integration of the Dirac equation has been started well within the nuclear regime. In the version of the method used here, the actual crystal unit cell is approximated by spheres around the atomic sites. As the crystal wave function in this geometry naturally is decomposed according to its angular momentum character, the content of electrons of s, p, d, etc. character within each sphere are convenient numbers by which to describe the electronic structure of the solid under study. These occupancy numbers are the reminiscence of the atomic effective occupancies Z_s and Z_p discussed above, but in the LMTO scheme they are not unique but always related to some specific sphere size. Thus, when we compare occupancy numbers of a Mössbauer atom in different solids, it is always with the reservation that the pertinent sphere radii need not be equal.

II. THE LMTO METHOD

Although the LMTO method is by now well established in solid-state physics, so far little attention has been paid to it by Mössbauer spectroscopists; therefore, a very concise review of the method will be reproduced here to facilitate the discussion of the results obtained in the following section. The method is thoroughly discussed in Refs. 17 and 18.

The Hamiltonian for a system of interacting electrons in a solid can be greatly simplified by the theorems of density-functional theory,[19,20] according to which all ground-state properties can be derived from the solutions of the one-particle Hamiltonian,

$$H(\mathbf{r})=-\nabla^2+V_{\rm ext}(\mathbf{r})+V_H(\mathbf{r})+V_{\rm xc}(\mathbf{r}) . \tag{2}$$

Here the potential is decomposed into the external $V_{\rm ext}$, the Hartree V_H, and the exchange-correlation $V_{\rm xc}$ parts; throughout this work we use the local-density approximation with the parametrization of $V_{\rm xc}$ as provided by Vosko, Wilk, and Nusair.[21]

In the LMTO method the wave functions for a given $\mathbf{k}$ point in the Brillouin zone are sought as a linear combination of Bloch sums of muffin-tin orbitals

$$\psi^{\mathbf{k}}(\mathbf{r})=\sum_L a_L^{\mathbf{k}}\sum_{\mathbf{R}} e^{i\mathbf{k}\cdot\mathbf{R}}\chi_L(\mathbf{r}-\mathbf{R}) . \tag{3}$$

Here $\mathbf{R}$ denotes the lattice points and L is a combined index, $L=(\mathbf{q},l,m)$, where $\mathbf{q}$ labels the atoms within the basis and l,m are the usual angular momentum quantum numbers.

To determine the muffin-tin orbitals χ_L, the true crystalline potential is replaced by a potential, which is spherically symmetric inside touching spheres centered on the atomic positions and constant in the remaining parts of space. Inside the muffin-tin sphere the basis function is expanded in spherical harmonics times a radial function ϕ_l and its energy derivative $\dot{\phi}_l$

$$\phi_l(r,E)=\phi_l(r,E_{vl})+(E-E_{vl})\dot{\phi}_l(r,E_{vl}) . \tag{4}$$

The radial function ϕ_l is obtained by solving the Dirac equation in the limit of zero spin-orbit coupling at an appropriately chosen energy E_{vl}.[18,22,23] Expansion (4) has proved accurate over ranges of order 1 Ry corresponding to typical valence-band widths in solids. The radial function has to be matched to the solutions outside the atomic spheres so that the resulting muffin-tin orbital χ_L is everywhere continuous and differentiable.

In the LMTO method the muffin-tin approximation is replaced by the atomic sphere approximation (ASA), in which the touching muffin-tin spheres are expanded a little to include all of space. The ASA improves on the muffin-tin approximation by allowing for a spatial variation of the potential in the whole unit cell, but the consequence is a violation of geometry. The conceptual and computational simplifications of the ASA are, however, significant. A first-order correction for the overlap of spheres has been derived by Andersen,[17] and this is applied throughout the present work. Furthermore, to diminish overlaps in relatively open structures, additional ("empty") spheres are introduced on high-symmetry interstitial sites.[24] Thus, the diamond structure of α-Sn, the NaCl structure of SnSb and SnTe, and the fluorite structure of $SnMg_2$ are all described in terms of an fcc lattice with four sites in the basis, cf. Table I.

The energy eigenvalues $E^{\mathbf{k}}$ and the coefficients $a_L^{\mathbf{k}}$ are obtained by numerical diagonalization of the secular equation

$$\sum_L (H_{L'L}^{\mathbf{k}}-E^{\mathbf{k}}O_{L'L}^{\mathbf{k}})a_L^{\mathbf{k}}=0 , \tag{5}$$

where

$$H_{L'L}^{\mathbf{k}}=\langle\chi_{L'}^{\mathbf{k}}\,|\,H\,|\,\chi_L^{\mathbf{k}}\rangle , \tag{6}$$

$$O_{L'L}^{\mathbf{k}}=\langle\chi_{L'}^{\mathbf{k}}\,|\,\chi_L^{\mathbf{k}}\rangle . \tag{7}$$

The elements of these matrices are easily evaluated; however, the expressions are rather lengthy (see Ref. 18 for a

TABLE I. Three different crystal structures all describable in terms of an fcc lattice with four spheres in the basis, at $\mathbf{q}_1=(0,0,0)$, $\mathbf{q}_2=\frac{1}{4}(1,1,1)$, $\mathbf{q}_3=\frac{1}{2}(1,1,1)$, and $\mathbf{q}_4=\frac{3}{4}(1,1,1)$, by letting different spheres be empty.

	α-Sn	SnTe	$SnMg_2$
$\mathbf{q}_1$	Sn	Sn	Sn
$\mathbf{q}_2$	Sn	empty	Mg
$\mathbf{q}_3$	empty	Te	empty
$\mathbf{q}_4$	empty	empty	Mg

complete listing). From the solutions $a_L^{\mathbf{k}}$ of (5) the crystal charge distribution can be calculated. This may be used to construct a new potential, or, if self-consistency has been achieved, the contact density may be determined.

In this work the basis of muffin-tin orbitals includes *s*, *p*, and *d* orbitals, i.e., nine orbitals per point in the lattice basis. The summation over **k** points in the Brillouin zone is performed by the tetrahedron method.[25,18]

III. BAND STRUCTURES

A. Grey tin

Grey tin or α-Sn is the stable allotrope of tin below 13 °C at normal pressure. The crystal structure is diamond with a lattice constant of 6.483 Å (at 90 K).[26] In Fig. 1 is displayed the self-consistent and scalar-relativistic band structure of α-Sn obtained by the LMTO method as sketched in the preceding section. Furthermore, a correction for the leading nonspherical component of the potential inside spheres was incorporated.[27] Figure 2 shows the partial densities of states.

The lowest valence band is almost entirely Sn *s*-like, and the second is also predominantly of Sn *s* character but with an admixture of Sn *p* character. The third and fourth bands are Sn *p*-like with some weight in the empty spheres.

The energy eigenvalues at a few key symmetry points of the Brillouin zone are listed in Table II, where also available experimental information is quoted together with two previous calculations of the α-Sn band structure, the self-consistent and nonrelativistic pseudopotential calculation of Srivastava,[28] and the fully relativistic orthogonal plane-wave (ROPW) but non-self-consistent calculation of Ref. 29. The experimental data on the α-Sn band structure are scarce, and the values of Table II may be subject to some uncertainty. The overall agreement of the present calculation with experiments is quite good. The largest

TABLE II. Energy eigenvalues in eV at Γ, X, and L for the α-Sn band structure. The present calculation is compared to the nonrelativistic pseudopotential (PP) calculation of Ref. 28 (PP) and the relativistic OPW calculation of Ref. 29 (ROPW). Experimental data are collected according to the present authors' estimates from the data published in (a) Ref. 30, (b) Ref. 29, and (c) Ref. 31. The values L_3' and X_1 are tentatively obtained by subtracting the L_3'-L_1 transition energy from the L_1 conduction state and adding the X_4-X_1 transition energy to the X_4 state. With the exception of the L_1 and Γ_2' states, spin-orbit splitting is not considered for the experimental data, but given for the two calculations, which we compare with.

	Present	PP	ROPW	Expt.
Γ_1	−10.52	−9.85	−10.59	
Γ_2'	−0.73	−0.30	−0.42	−0.3,[a] −0.16[e]
Γ_{25}'	0.00	−0.87 0.00	−0.65 0.00	0.00
Γ_{15}	2.51	2.05 2.75	1.96 2.43	2.6[b]
X_1	−7.59	−7.04	−7.59	−7.5(5)[c]
X_4	−2.47	−2.15	−2.43	−2.8(1)[c]
X_1	1.11	1.62	0.97	0.7[d]
L_2'	−9.02	−8.16	−9.07	
L_1	−6.33	−5.56	−6.28	
L_3'	−1.15	−1.41 −0.75	−1.39 −0.98	−1.3[d]
L_1	0.08	0.58	0.15	0.09,[a] 0.32[e]

[a]Reference 30.
[b]Reference 29.
[c]Reference 31.
[d]The transition energies of Ref. 32 are used.
[e]Same as Ref. 30, but spin-orbit corrected (Ref. 33).

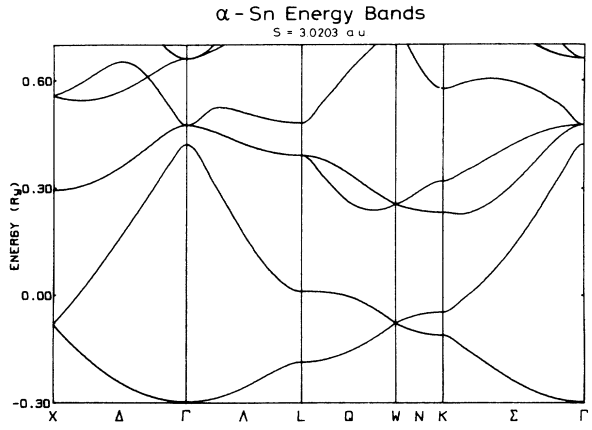

FIG. 1. Scalar-relativistic band structure of α-Sn.

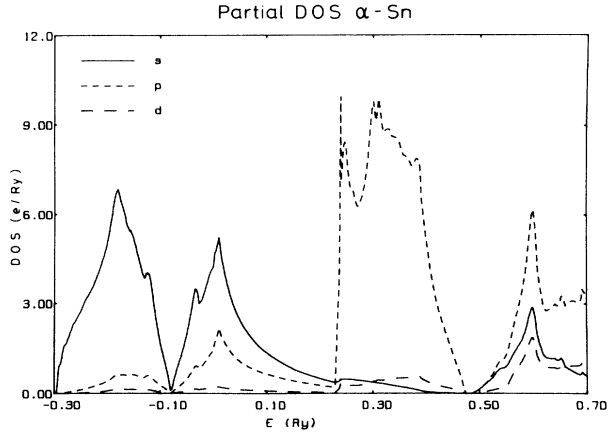

FIG. 2. Partial densities of states of α-Sn.

discrepancy is in the upper valence band in the Δ direction, where the angle-resolved photoemission spectroscopy (ARPES) measurements of Ref. 31 yield a somewhat larger dispersion than exhibited by the calculated bands. The calculated position of the somewhat troublesome Γ_2' state is too low by ~ 0.6 eV, but this is a general feature of local-density-approximation (LDA) calculations of tetrahedral semiconductors also encountered in Si, Ge, and GaAs.[34,23] The indirect gap at Γ_{25}'-L_1 comes out quite small but positive in accordance with experiment.

Considering the other two calculations quoted in Table II, a striking agreement between the results of the present calculation and the ROPW calculation of Ref. 29 is noted. Except for the Γ_2' state, all energies of both valence and conduction states are equal to within 0.1 eV. This is rather surprising, since the effective crystal potential used in Ref. 29 was a superposition of overlapping atomic potentials, which are relativistic, self-consistent, and included exchange through the Kohn-Sham parametrization of the LDA. However, the crystal potential itself was not iterated to self-consistency, and as it is generally important to do this, the accordance of the two calculations is indeed puzzling. The positions of the Γ_{15}, X_1, and L_3 conduction states are calculated to be somewhat higher in the present work than in Ref. 29. This is probably due to the overestimation of the nonspherical potential variation inherent in the present approach.[27]

The calculation of Srivastava[28] did iterate the crystal potential to self-consistency, but did not include relativistic effects (except spin-orbit coupling). The general trends of scalar relativistic effects, discussed in Ref. 23, may therefore be recognized by comparing with the present calculation: The lowest valence band drops by 0.8 eV when scalar-relativistic effects are included [as compared to 0.3 eV for Ge and GaAs (Ref. 23)], and all the conduction states likewise shift downwards, most the L_1 and X_1 states. Also the Γ_2' is lowered, though surprisingly only by 0.4 eV, whereas the antibonding s state in Ge and GaAs was seen to drop more than the bonding Γ_1 state.[23]

B. White tin

White tin or β-Sn is the stable form of tin at temperatures above 13 °C at zero pressure. The β-Sn crystal structure is body-centered tetragonal with a two-atomic basis of coordinates $\mathbf{q}_1=(0,0,0)$ and $\mathbf{q}_2=(a/2,0,c/4)$ and a flat conventional cell with $a=5.812$ Å and $c/a=0.5433$.[35] Tin is the only element that crystallizes in this structure at ambient conditions.

The β-Sn structure fits naturally into the general trend of greater metallicity or less covalency as one passes down the group IV of the Periodic Table. The lighter elements C, Si, and Ge all crystallize in the diamond structure—with experimental band gaps of 5.4, 1.2, and 0.75 eV respectively—whereas the heavier Pb is fcc and metallic. Sn in the α-Sn phase is a semimetal with an exactly vanishing band gap. β-Sn may be looked upon as a large distortion of the α structure by a uniaxial compression along the z (or c) axis accompanied by an expansion in the xy plane. The number of nearest neighbors is still four—at positions $(\pm a/2,0,c/4)$ and $(0,\pm a/2,-c/4)$ at a distance 3.02 Å away—but the ideal tetrahedral angle of 109.5° is now replaced by angles of 94.0° and 149.5° between the directions of nearest neighbors. Furthermore, two next-nearest neighbors at $(0,0,\pm c)$ are only slightly more distant (3.18 Å), making the effective coordination closer to six.

Si and Ge are known to undergo phase transformations into the β-Sn structure upon application of hydrostatic pressures around 125 and 110 kbar, respectively,[36] and a similar transformation has been predicted for C at 12 Mbar,[37] a pressure by far beyond present experimental capability. The symmetry properties of the β-Sn point group D_{4h}^{19} have been discussed by Miasek and Suffczynski.[38]

β-Sn is somewhat more close packed than α-Sn; touching spheres will cover 53% of space as compared to α-Sn 34% and fcc 74%. One may therefore hope to be able to perform an LMTO calculation of β-Sn without introducing empty spheres to fill out space (anyway, there is no obvious high-symmetry interstitial site, where an empty sphere seems suitable). To cover a volume equal to the actual crystal volume by atomic spheres, we must expand the touching spheres by 23%, whereby the total volume inside overlap regions amounts to $\sim 13\%$, which is somewhat worse than in the diamond structure with empty spheres. The atomic radius thus becomes 3.51 a.u.

The self-consistent scalar-relativistic band structure of β-Sn calculated with this approach is presented in Fig. 3, and the valence-band density of states with the s, p, and d components projected out are presented in Fig. 4. The calculations presented used a mesh of 130 **k** points in the irreducible wedge of the Brillouin zone. The two lowest valence bands are seen to practically separate from the upper ones. They are the bonding and antibonding s bands, whereas the upper valence bands are predominantly of p character. There is no gap between the s and p bands, but a marked depletion in the density of states is seen in the region from -0.10 to 0.15 Ry in Fig. 4.

Very few calculations of the band structure of white tin have been reported in the literature. Miasek[38] used the OPW method for calculating the band structure in selected **k** points. Weisz[39] used a semiempirical pseudopotential method fitting the pseudopotential form factors to get

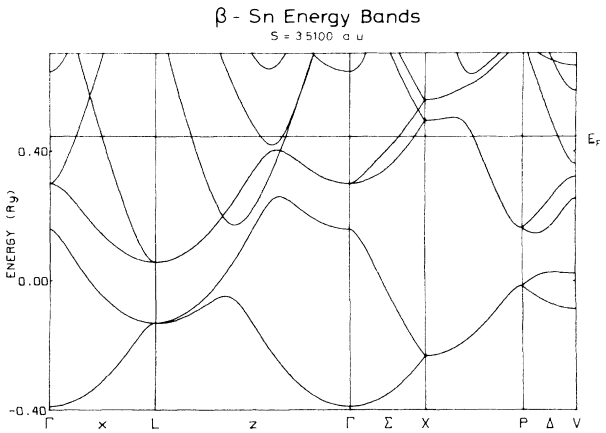

FIG. 3. Scalar-relativistic band structure of β-Sn.

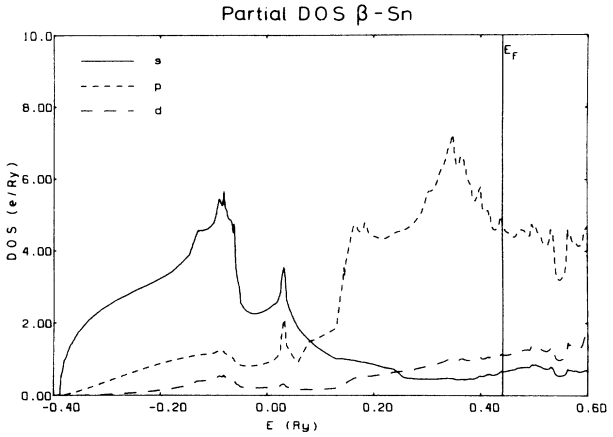

FIG. 4. Partial densities of states in β-Sn.

a Fermi surface consistent with experiments. Craven[40] repeated this calculation a few years later and found good quantitative agreement with de Haas—van Alphen experiments. Ament and de Vroomen[41] have done a fully relativistic augmented plane-wave (APW) calculation using the $X\alpha$ scheme for exchange and correlation effects; however, it was not iterated to self-consistency. Finally, Ihm and Cohen[42] did a self-consistent nonrelativistic pseudopotential calculation to study the phase transition $\alpha \rightarrow \beta$. In the present work we both iterate the crystal potential to self-consistency and include all relativistic effects, except spin-orbit coupling. The effects of spin-orbit interaction are of the order of 0.5 eV in the band energies,[40] and as some of the degeneracies of the scalar-relativistic bands will be lifted, they are rather important for a detailed discussion of the complicated Fermi surface. This will not be attempted here. Also, some of the band crossings in Fig. 3 will be forbidden.

In Table III we compare the present calculation with the relativistic APW (RAPW) calculation of Ref. 41. There is a general agreement on the topology of the energy bands and the typical quantitative discrepancies on the energy eigenvalues are of the order 0.1—0.2 eV. Both of the semiempirical pseudopotential calculations of Refs. 39 and 40 are significantly at variance with those of Table III.

TABLE III. The energy eigenvalues at selected symmetry points for β-Sn. The present work is compared to the RAPW calculation of Ref. 41. All values are in eV and relative to the Fermi level.

	Present	RAPW
Γ_1^+	−11.34	−11.3
Γ_1^-	−3.90	−3.7
Γ_5^+	−1.97	−2.0
Γ_4^-	2.71	2.9
X_1	−9.21	−9.0
L_2	−7.83	−7.7
L_3	−5.28	−5.0
P_2	−6.26	−6.0
P_1	−3.84	−3.6

The only experimental information which we are able to use for comparison is a measurement of the density of states by x-ray photoelectron spectroscopy (XPS).[43] The experimental resolution is not comparable to the computer's, but the three main peaks of Fig. 4—at 520, 410, and 95 mRy below the Fermi level—are easily resolved. The experimental values are[44] ~0.50, 0.41, and 0.11 Ry, respectively, in excellent agreement. Also, the depletion between s and p bands is easily seen, and a width of this region of ~0.25 Ry is estimated, in accordance with Fig. 4.

C. Tin telluride and tin antimonide

The binary compounds of tin with its nearest neighbors in columns V and VI of the Periodic Table, antimony and tellurium, are of considerable interest in the context of Mössbauer experiments. This stems from the fact that ^{121}Sb and ^{125}Te also are important Mössbauer isotopes. It is a powerful check of the reliability of the adopted calculational scheme that we are able to extract from the same calculation two quantities, which can be compared to independent experimental isomer shifts.

SnTe belongs to the class of binary compounds of elements from groups IV and VI of the Periodic Table, which also comprises the salts of Pb with S, Se, and Te. These materials show peculiar properties in being narrow-gap semiconductors with a direct gap at the L point of the Brillouin zone. For a general review of these materials, see Ref. 45.

SnSb and SnTe have, respectively, nine and ten valence electrons per molecule. This does not favor the tetrahedral coordination, which is so strongly dominant when eight valence electrons per molecule are present. Rather, the bonding properties of SnTe, being isoelectronic with Sb, are very similar to that of this element. Thus, as Sb in the arsenic structure may be thought of as a distorted simple cubic arrangement, SnTe is found in a rhombohedral crystal structure, which constitutes a very slight distortion of the NaCl structure, the binary analog of the simple-cubic structure. In the NaCl structure each atom is surrounded by six nearest neighbors of the opposite kind, at the apices of an octahedron, and the p orbitals provide bond orbitals favoring exactly this symmetry. However, due to a slight hybridization with s and d orbitals, a small distortion occurs. The distortion of the ideal NaCl structure is, however, much less than the analogous distorted simple-cubic structure of antimony. The cubic right angles thus change into 89.88° in SnTe,[46] and at temperatures above about 160 K the ideal NaCl structure is actually stable.[47]

Similar behavior is encountered for SnSb, though the atoms of this compound do not in their free ground state have the appropriate number of p electrons to occupy all bonding p orbitals. For this reason some degree of promotion of the metallic s electrons into covalent bond orbitals must be expected with an associated influence on the electron contact density. The distortion of the NaCl lattice is given by the bond angle in this case being 89.7°,[48] and it is preserved also at elevated temperatures.

The reason for the much smaller distortion of the ideal cubic lattice seen with SnTe and SnSb in comparison with Sb is the slight ionic character of the bonds, which accompanies the difference in the electronegativity of the Sn atom and its ligand and tends to stabilize the ideal cubic arrangement.[49] The fact that the bonds in SnTe and SnSb are both ionic and covalent in character is also revealed in the nearest-neighbor distances being 3.16 and 3.07 Å, respectively, which is midway between the sum of the covalent radii —2.77 and 2.81 Å—and the sum of the ionic radii—3.33 and 3.38 Å.[50]

In this subsection we report on calculations of the electronic structure of SnTe and SnSb, disregarding the tiny distortion of the ideal NaCl structure just discussed. This approximation should not have any large influence on the electronic structure. For the lattice constants we have taken $a=6.130$ Å and $a=6.313$ Å, for SnSb and SnTe, respectively.[51] Empty spheres were included in the way described in Table I.

The self-consistent scalar-relativistic band structures of SnTe and SnSb are depicted in Figs. 5 and 6 with the densities of states in Figs. 7(a) and 7(b) and 8(a) and 8(b). The SnTe bands are recognized as the Te s band lowest, separated from the second band, the Sn s band by ~ 4 eV, while the next three are the bonding p bands with their main weight inside the Te spheres but with appreciable Sn p character as well. Some Sn s admixture is also seen for the highest states of the fifth band. The empty spheres have their dominating weight within the p bands. A tiny gap is seen to open up at the L point, i.e., SnTe turns out a narrow-gap semiconductor in accordance with experimental facts. A secondary direct gap appears along the Σ line from Γ to K. In contrast to the zinc-blende structured semiconductors, the Γ point has ceased to be peculiar in any respect.

The SnSb bands look very much like the SnTe bands, but the nine electrons per unit cell make SnSb a genuine metal with a complicated Fermi surface. The first band is the Sb s band, which appears wider than the Te s band in SnTe, and also less separated from the second band, which is seen to be predominantly of Sn s character, but now with some Sb s and p admixture. Also, this band is wider, by ~ 2 eV, than its counterpart in SnTe. The three bonding p bands are again seen to involve some Sn s mixing, especially in the portion above the Fermi level. There is no gap at L between the fifth and the sixth bands, as the doubly degenerate L_3 state now appears to be lowest. Also, the Σ gap has almost closed.

The band structure of SnTe has been investigated theoretically in a number of publications mainly driven by

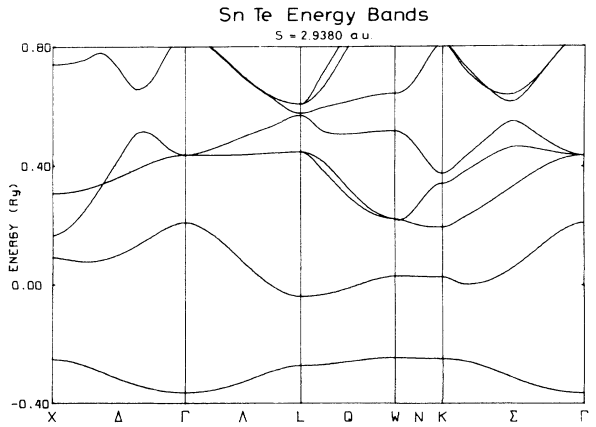

FIG. 5. Scalar-relativistic band structure of SnTe.

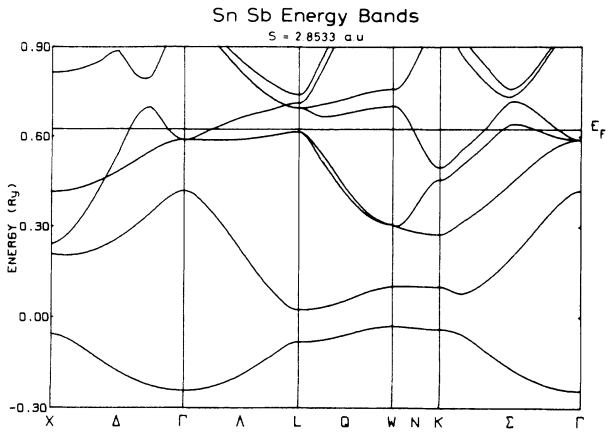

FIG. 6. Scalar-relativistic band structure of SnSb.

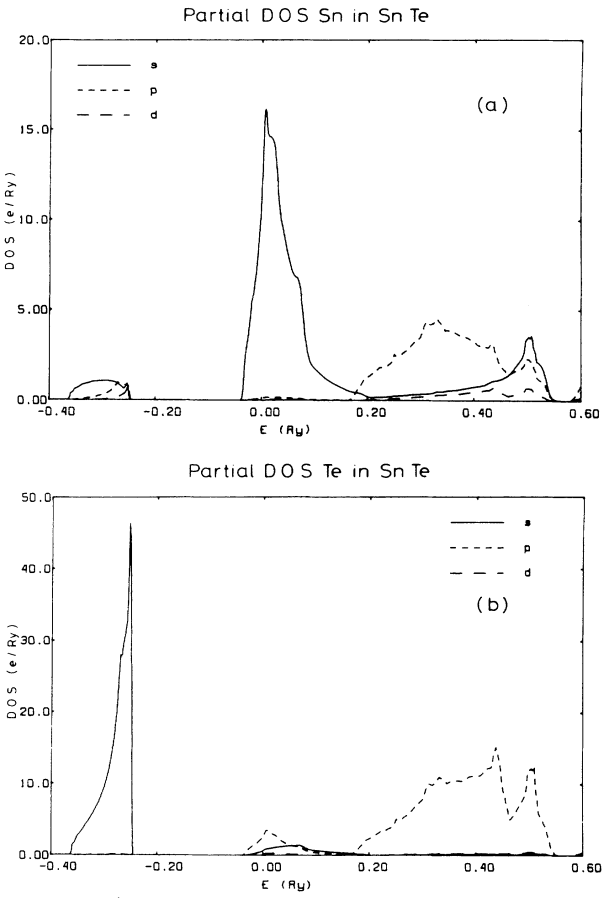

FIG. 7. (a) Sn partial densities of states in SnTe. (b) Te partial densities of states in SnTe.

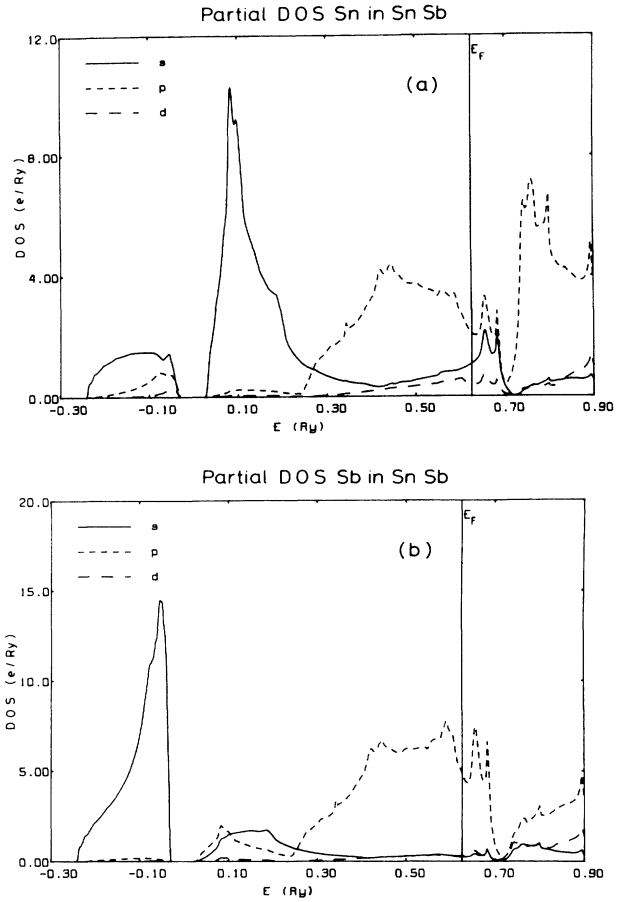

FIG. 8. (a) Sn partial densities of states in SnSb. (b) Sb partial densities of states in SnSb.

the anxiety to get a consistent picture of the energy levels around the gap. Herman *et al.*[52] performed a relativistic OPW calculation and Rabii[53] an APW calculation, without iterating the crystal potential to self-consistency. Tung and Cohen[54] and Bernick and Kleinmann[55] have employed the empirical pseudopotential method, and Robertson[56] employed a parametrized tight-binding method. The only self-consistent calculations previously reported appear to be the relativistic APW calculation of Melvin and Hendry[57] and the recent relativistic pseudopotential calculation of Rabe and Joannopoulos.[58] Both of these references use the Baldereschi special-points method[59] for obtaining the crystal charge density. Melvin and Hendry used only three special points and concluded that the effects of spin-orbit coupling indeed are rather small compared to the scalar-relativistic effect. However, precise spin-orbit coupling caused a gap to open up at the L point, their scalar-relativistic calculation finding SnTe a semimetal, and is therefore of a distinct qualitative influence. As mentioned, the scalar-relativistic calculation of this work does produce a gap at L, as did that of Rabe and Joannopoulos.[58]

In Table IV are listed the eigenvalues at the high-

TABLE IV. Band energies of SnTe and SnSb at selected symmetry points in eV (relative to valence-band top for SnTe and Fermi level for SnSb). The SnTe calculation is compared with the RAPW calculation of Ref. 57 and experimental information.

	SnTe			SnSb
	Present	RAPW	Expt.	Present
Γ_1	−12.71	−12.3		−11.80
Γ_1	−4.91	−4.4		−2.79
Γ_{15}	−1.81	−1.6		−0.47
Γ_{15}	3.76	3.5		5.00
X_1	−11.20	−10.9		−9.26
X_1	−6.48	−6.2		−5.66
X_4'	−5.50	−5.1	−5.0(3)[a]	−5.22
X_5'	−3.59	−3.1	−2.6,[a] −2.9[a]	−2.85
X_3	2.31	2.0		2.58
L_2'	−11.47	−11.2	−11.9,[a] −11.6[b]	−9.60
L_1	−8.28	−7.9		−8.16
L_3	−1.66	−1.3		−0.12
L_2'	0.00	0.0		1.19
L_1	0.10	0.0	0.35[c]	1.57
L_3'	0.52	0.9		0.97
Σ_{max}	−0.27	−0.07	−0.07[c]	

[a]Reference 60.
[b]Reference 61.
[c]Reference 62.

symmetry points Γ, X, and L for the two LMTO calculations of this work. The results of Melvin and Hendry[57] are likewise quoted for comparison, as are the experimental SnTe data available. Neither experimental nor theoretical data on the band structure of SnSb seem to have been published. Experimental data on SnTe stem from photoemission studies providing a mapping of the density of states. However, assigning specific structures of this to certain band extrema is rather difficult. It is sufficient to say that the identifications of the table agree with the calculations to within 1 eV. For the experimental information concerning the gaps, namely the direct L_2'-L_1 and the position of the second valence-band maximum along the Σ line, we get excellent agreement when considering the fact that spin-orbit coupling is not included in the calculation. Actually, the true valence-band maximum and conduction-band minimum are not exactly at the L points, but at points on the hexagonal face 3—4 % of the distance towards the W points. Here other calculated gap has shrunk to 0.02 eV. This peculiar gap structure of SnTe agrees with the experimental picture[62] as well as with other calculations.[57,63]

Comparing the SnTe calculation with the relativistic and self-consistent APW calculation of Melvin and Hendry,[57] a systematic trend is observed, as the valence-band energies of the present work fall 0.2—0.5 eV below those of Ref. 57. We have no explanation for this but note that a downwards shift of the upper L_2' and L_1 states by 0.3

eV in the present work will bring the two calculations in perfect agreement.

D. $SnMg_2$

$SnMg_2$ is in many respects similar to the zinc-blende-structured compounds. This is due to the number of valence electrons being eight per molecule in both cases. Sn provides four electrons, in the atomic ground-state configuration $5s^25p^2$, and each Mg provides two electrons with the $3s^2$ atomic ground-state configuration. The crystal structure of $SnMg_2$ is fluorite, which—as mentioned in Sec. II—is very similar to the zinc-blende structure: The tin atoms occupy a fcc sublattice, while the Mg occupy *two* fcc sublattices displaced, respectively, $\frac{1}{4}$ and $-\frac{1}{4}$ of the body diagonal relative to the Sn lattice. Each Mg atom is therefore surrounded by four tin atoms in the same tetrahedral coordination as found with the zinc-blende compounds. Thus, the formation of sp^3 orbitals on the Mg atoms appears favorable. However, each tin atom is surrounded by eight Mg atoms at the corners of a cube; this high coordination rather favoring metalliclike bonding on the Sn atoms.

The self-consistent scalar-relativistic band structure of $SnMg_2$ is depicted in Fig. 9 with the partial density of states in Figs. 10(a) and 10(b). The calculation used equal radii of all constituent spheres.

The band structure of Fig. 9 is indeed very similar to that of the zinc-blende semiconducting compounds. The maximum of the valence bands is at Γ, while the minimum of the conduction bands is found at X (in the present calculation the X_3 conduction state actually dips below the valence-band maximum). From the l-projected density of states, Figs. 10(a) and 10(b), the first valence band is recognized as the Sn s band. The second band has mixed Sn p and Mg s character, whereas the upper two are predominantly Sn p-like with some Mg p admixture. The first conduction band appears to have mostly Mg s and p character.

The only previously reported calculations of the band structure of $SnMg_2$ that we are aware of are two empirical pseudopotential calculations.[64,65] In Table V the present

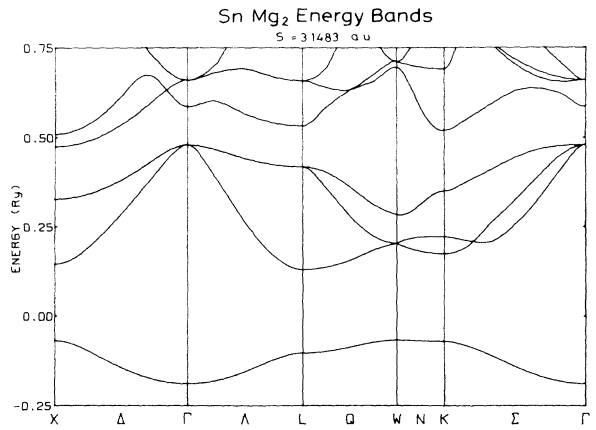

FIG. 9. Scalar-relativistic band structure of $SnMg_2$.

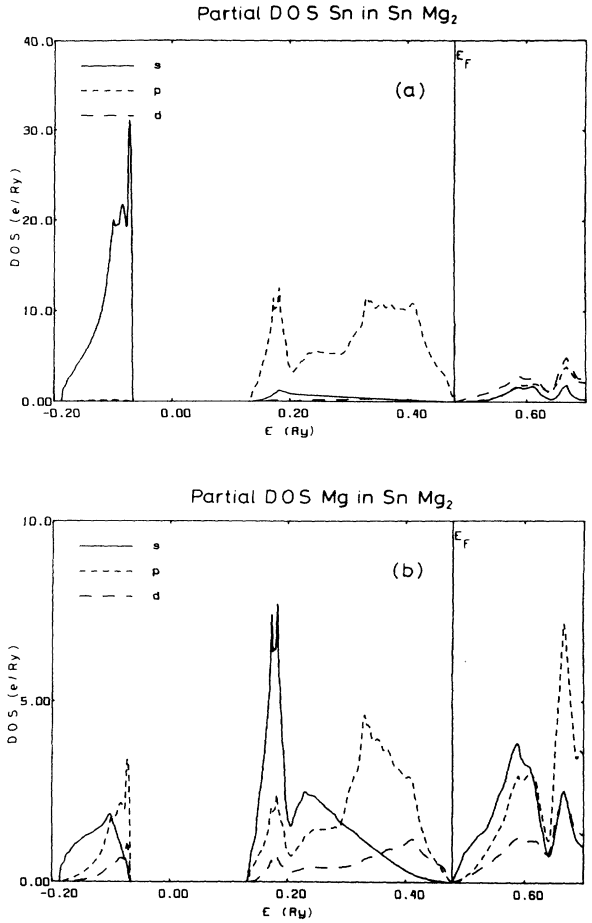

FIG. 10. (a) Sn partial densities of states in $SnMg_2$. (b) Mg partial densities of states in $SnMg_2$.

calculation is compared to that of Ref. 64. Experimental information on $SnMg_2$ is scarce. UPS (Ref. 66) and XPS (Ref. 67) measurements of the valence-band density of states are able to resolve the three main peaks of Figs. 10(a) and 10(b) stemming from the first, second, and third and fourth bands, respectively. According to Ref. 66, the peak tops are located at 8.5, 4.3, and 1.4 eV below the top valence state, whereas our calculation gives 7.9, 4.0, and 1.6 eV, respectively, so the agreement is good.

Concerning the fundamental gap of $SnMg_2$, experimental information is also limited. According to Ref. 68 the gap is indirect of magnitude 0.185 eV, while another conduction-band minimum is found at 0.35 eV above the valence-band edge. This gap is often quoted as the minimum direct gap of $SnMg_2$, though the original reference[68] states that it can be situated anywhere in the Brillouin zone. The calculation of this work indeed gets the minimum conduction state off the zone center at X, where, as mentioned, the fifth band actually dips below the valence-band edge, making the calculated $SnMg_2$ crystal a semimetal. However, this is no more peculiar than what is encountered with other semiconductors and is due

TABLE V. $SnMg_2$ energies at symmetry points compared to those obtained by the empirical pseudopotential method (EPM) in Ref. 64. At K only the lowest conduction state is given. All values are in eV relative to the top valence state at Γ.

	Present	EPM
Γ_1	−9.10	−8.5
Γ_{15}	0.00	0.0
Γ_1	1.44	1.8
Γ'_{25}	2.44	2.4
X_1	−7.45	−6.9
X'_4	−4.56	−4.3
X'_5	−2.09	−2.0
X_3	−0.07	0.2
X_1	0.40	0.6
L_1	−7.93	−7.3
L'_2	−4.76	−4.5
L'_3	−0.84	−0.8
L_1	0.71	0.9
L_3	2.41	2.4
K_1^c	0.54	0.7

to the manifest shortcoming of the LDA in the description of the band gaps of semiconductors.[23,34,69] The next conduction-band edge of the present calculation also appears at X, about 0.4 eV higher than the valence-band maximum. Other edges are at K and L at 0.5 and 0.7 eV above the valence bands, but the minimum direct gap, at Γ, is 1.4 eV. Thus, we must conclude that the next conduction-band edge cannot be at Γ but most probably at X with L and K as other possibilities. The quantitative separation between the conduction-band edges is not well produced in our calculation and spin-orbit coupling must be considered before better agreement can be expected.

The above findings are in agreement with those of Refs. 64 and 65. For the lower valence states the empirical pseudopotential method generally gets higher energy levels, which may be due to the relativistic effects incorporated in the present work.

E. Tin dioxide

The SnO_2 crystal structure is rutile, which is a simple tetragonal lattice with two formula units per unit cell. Each Sn atom is surrounded by six oxygens in a distorted octahedral coordination. Due to the distinct ionic character of this compound, it is of considerable interest in connection with the calibration of Mössbauer isomer shifts.

The LMTO band structure of SnO_2 has been discussed in a previous publication.[70] Some qualitative experimental facts are not reproduced, notably the direct character of the band gap and the symmetry properties of the topmost valence state at the zone center, but quantitatively the discrepancies are not large. The calculations used equally large spheres for Sn and O, which makes it possible to contain the Sn^{4+} core within the sphere as well as the valence-electron charge cloud of a negatively charged oxygen ion. Unfortunately, larger overlaps result from this choice, which may account for the discrepancies mentioned.

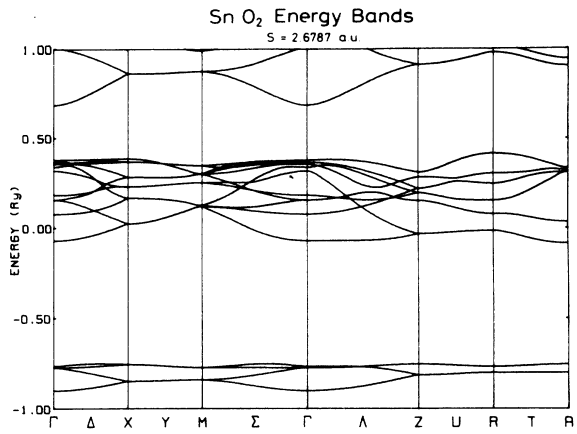

FIG. 11. Scalar-relativistic band structure of SnO_2.

The SnO_2 band structure is displayed in Fig. 11 and the partial density of states in Figs. 12(a) and 12(b). From these figures we recognize the four deep-lying corelike oxygen s-bands and the 12 valence bands of predominantly

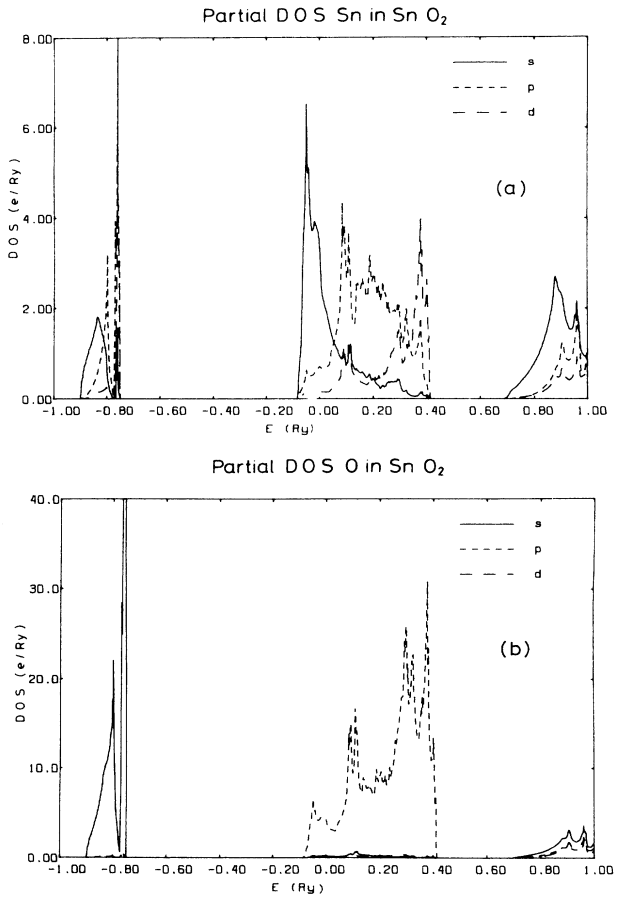

FIG. 12. (a) Sn partial densities of states in SnO_2. (b) O partial densities of states in SnO_2.

O p character. However, there appears to be a significant admixture of Sn s character into the O s bands and lower valence region, and Sn p and d character into the upper valence bands. Thus, a significant degree of covalency is present in the SnO_2 crystal[70] with substantial impact on the interpretation of Mössbauer isomer shifts, as will be discussed in Sec. IV.

IV. THE ELECTRONIC STRUCTURE

In Table VI are listed the key quantities describing the electronic configuration at the Sn containing crystals. These comprise the electron contact density at the Sn nucleus and the decomposition of the crystal wave function into angular momentum character inside the sphere around the Sn nucleus, the radius of which is also given. The experimental values[71,72] of the isomer shifts relative to a SnO_2 source are likewise given. For SnSb and SnO_2 the results of two calculations are listed. The calculation of SnSb with $S=2.85$ a.u. used this sphere size for all constituent spheres, i.e., for the Sb sphere and the empty spheres as well, whereas the second calculation kept the same total crystal volume but chose the radius of the Sn and Sb spheres 20% larger than the empty spheres, at 3.09 a.u. Similarly, for SnO_2 one calculation used equally large Sn and O spheres with $S=2.68$ a.u., while the second calculation adopted the oxygen radius 10% larger than the tin radius, but the same total volume. These additional calculations were only aimed at getting the occupancies pertinent to different Sn sphere sizes, but did not use enough **k** points in the Brillouin-zone sampling to obtain a converged electron contact density. All other calculations used equally large spheres for all constituents.

In α-Sn the s-electron content within the Sn sphere is 1.41 electrons. This is somewhat larger than the 1.35 and 1.19, which have been derived for Ge and Si in completely analogous calculations[73] illustrating the trend of increasing metallicity on descent down group IV of the Periodic Table. Antoncik[74] has calculated the number of s electrons in Si, Ge, and α-Sn from a tight-binding scheme to be 1.35, 1.50, and 1.56, respectively. These numbers refer to a geometry without empty spheres and are not directly comparable to the occupancy numbers of the present work, but they appear to be consistently 0.15 higher. The widely anticipated valence-electron structure of Sn as s^1p^3 is seen to be far from correct. The dehybridization of the sp^3 bond orbitals increases down the group IV due to the larger promotion energy, which accompanies the larger atomic volume. This dehybridization is quite significant in Ge and α-Sn, and in the next element, Pb, it is complete, as this element is not found in any covalent crystal structure. The sp^3 picture is only a qualitative concept referring to the symmetry of the diamond crystal structure, but the extent to which the electronic Bloch wave functions build up their amplitude in the bond regions is a matter of tradeoff between the depth of the potential here and the depth of the potential well around the constituent atoms.

A direct comparison of the occupancy numbers of β-Sn with those of α-Sn is hindered due to the fact that empty spheres were used in the α-Sn calculation but not in the β-Sn calculation. However, the electron contact density is found to be larger in β-Sn in accordance with the anticipation that this phase is more metallic and therefore has more s-electron character in the wave function. The configuration of a Sn atom in β-Sn is found to be $s^{1.62}p^{2.04}d^{0.34}$, which may be compared to the results of Ref. 75. These authors performed an analysis of the chemical shifts of the $3d$ core levels of α-Sn and β-Sn and combined it with Mössbauer isomer shifts and with results of internal conversion measurements to estimate an s-occupancy number of β-Sn of $n_s=1.6\pm0.3$, while the change in s occupancy in going from the α phase to the β phase was found to be $\Delta n_s(\alpha-\beta)=0.1-0.2$ electrons. These numbers are in excellent agreement with the present calculations and constitute an encouraging experimental confirmation of the results of the present calculations.

The sequence of α-Sn, SnSb, and SnTe may be looked upon as a series of binary alloys of tin with the neighboring elements of $Z=50$, 51, and 52. As discussed in Sec. III C, the diamond structure is only favorable when eight valence electrons per unit cell are present as in α-Sn, whereas SnSb and SnTe with nine and ten valence electrons crystallize in (a slightly distorted version of) the NaCl structure, whose symmetry is that of pure p orbitals. In SnTe the number of p electrons supplied by the atoms exactly saturates the available bonding p orbitals, so that no promotion of s electrons takes place. The Sn s occupancy is consequently higher in SnTe than in α-Sn. The Sn p electron content is low in SnTe, indicating that a large transfer has occurred, mainly into the empty spheres, which do not to the same extent represent

TABLE VI. The experimental isomer shift (Δ_{IS} in mm/sec relative to a SnO_2 source) together with calculated quantities describing the electronic structure of the tin compounds. S is the radius of the sphere around the tin nucleus in atomic units, $\rho(0)$ is the electron contact density of Sn in atomic units (a_0^{-3}), and n_l the number of electrons of angular momentum character l within the Sn sphere.

	α-Sn	β-Sn	SnSb		SnTe	$SnMg_2$	SnO_2	
Δ_{IS}	2.012(12)	2.542(5)	2.77(2)		3.460(15)	1.860(5)	0	
S	3.02	3.51	2.85	3.09	2.94	3.15	2.68	2.51
$\rho(0)$	62.33	65.64	69.45		78.64	59.46	30.3	
n_s	1.41	1.62	1.39	1.52	1.57	1.46	0.69	0.57
n_p	1.77	2.04	1.19	1.43	1.00	2.35	0.94	0.71
n_d	0.13	0.34	0.12	0.20	0.12	0.05	0.44	0.31

charge-depleted regions as is the case with the empty spheres in the diamond structure. The increased s content and decreased p content of the Sn sphere in conjunction lead to a large value of the electron contact density of Sn in SnTe.

The charge cloud of Sn in SnSb does not have as much s character as its counterpart in SnTe. Thus, if we interpolate between the two calculations of SnSb quoted in Table VI to a sphere volume equal to that used for Sn in SnTe, we may estimate the occupancy numbers of this sphere to be $n_s=1.44$, $n_p=1.26$, i.e., 0.13 s electrons fewer than seen in SnTe. This suggests that some degree of promotion into bonding p orbitals has taken place, as the atomic p electrons do not by themselves saturate the bond orbitals. The accompanying increase in Sn p electron content in SnSb reflects the smaller ionicity of this compound, and both of these trends account for the lower Sn electron contact density in SnSb in comparison with SnTe. However, the s-electron occupancy is still higher in SnSb than in α-Sn, indicating that the aforementioned promotion of s electrons is not as pronounced in SnSb as in α-Sn. Also, the α-Sn crystal is not ionic, giving rise to larger Sn p-electron content in this material.

$SnMg_2$ is the only tin compound considered in this work, where tin takes on the role of the anion. Comparing the occupancy numbers of this compound with those of α-Sn, practically the same s-electron content is seen, around 1.4. A slightly larger s-electron content in $SnMg_2$ would be in accordance with the eight-fold coordination of the Sn atom in this compound, which favors the metallic nondirectional bonding more. It is not possible to tell from the quoted numbers whether this is the case, as the different volumes of the respective Sn spheres blur the picture. However, it is evident that the Sn sphere of $SnMg_2$ has accommodated more p electrons than its counterpart in α-Sn, the difference being around 0.6 electrons. This reflects the larger electronegativity of Sn in comparison with Mg, causing a charge transfer towards the Sn atom. The charge pileup on Sn is mainly in the outermost regions of the sphere having p character. Thus, it can be concluded that the lower electron contact density of $SnMg_2$ in comparison with α-Sn is a consequence of the increased shielding of the s electrons away from the nuclear region, which is mediated by the larger p-electron charge cloud. This effect may be somewhat reduced by a slightly higher s-electron occupancy of Sn in $SnMg_2$.

Finally, the rutile-structured SnO_2 compound shows distinct ionic properties. Thus, the electron contact density is roughly half the value seen in α-Sn and the occupancies show 0.6—0.7 s electrons around Sn, to be compared with the 1.4 s electrons of α-Sn. The total electron content of the Sn sphere is 2.1 and 1.6 for the two sphere choices adopted, showing that a large amount of charge has been dragged away from the Sn atom and towards the O atom. On the other hand, it is far from the total valence charge of 4 that has left, demonstrating that a significant degree of covalency is present in the bonding of rutile SnO_2.

The experimental isomer shifts are plotted against the calculated valence electron contact densities in Fig. 13. The linearity is very good. As the experimental data are

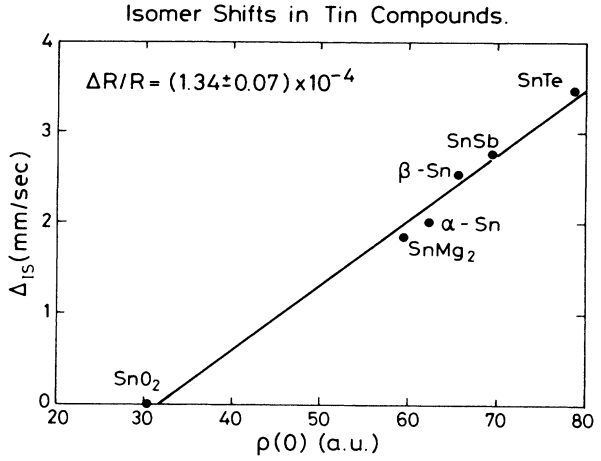

FIG. 13. The experimental isomer shifts of the Sn compounds plotted against the calculated valence-electron contribution to the electron contact density.

so accurate, the deviations from linearity indicate the magnitude of calculational fluctuations. From a least-squares fitting we get a value for the relative change in nuclear radius of

$$\frac{\Delta R}{R}=(1.34\pm0.07)\times10^{-4}\,. \tag{8}$$

The calibration of the ^{119}Sn resonance has been attempted by many authors. A recent compilation of the nuclear calibration factor obtained in previous works may be found in Ref. 13. Ignoring the earliest crude estimates, it is probably safe to say that values of $\Delta R/R$ seem to converge towards a value in the range $\Delta R/R=(0.7-1.8)\times10^{-4}$. Our value (8) is in excellent agreement with this, falling right in the middle. The methods used for calibration generally fall in two groups. The first group follows the same strategy as here, i.e., compares measured isomer shifts to calculated electron contact densities derived from more or less sophisticated schemes. The second group attempts to derive an independent experimental value of the electron contact density with which to compare the Mössbauer isomer shifts. The internal conversion of valence electrons in a solid is used, but large experimental difficulties prevail. It is, however, encouraging to see the general agreement on the value of the calibration constant obtained by these two approaches. The attempts to calculate the change in nuclear radius between the excited- and the ground-state level from first principles using some model for the nuclear state are scarce and the accuracy limited.

The pressure dependence of the isomer shift of the ^{119}Sn resonance in β-Sn has been investigated by the present authors in a previous publication.[76] In the present work we have also varied the volume of α-Sn to get (via the Pettifor pressure formula)[77,18] predictions for the equilibrium lattice constant and bulk modulus, as well as

TABLE VII. Calculated and experimental lattice parameter, a in Å, bulk modulus B in Mbar, and volume derivative of the electron contact density, in a_0^{-3}, for α-Sn and β-Sn.

		a	B	$\frac{d\rho(0)}{d\ln V}$
α-Sn	calc.	6.528	0.51	14.2
	expt.	6.483[a]	0.53[b]	
β-Sn	calc.	5.588	0.57	12.8
	expt.	5.812[c]	0.579[c]	14.5(5)[d]

[a]Reference 26.
[b]Reference 78.
[c]Reference 34.
[d]Experimental value of $d(\Delta_{IS})/dP$ from Ref. 79 converted by $\Delta R/R$ value of Eq. (8) and the average bulk modulus $\overline{B}=0.72$ Mbar in a 0—100 kbar range.

TABLE VIII. Electron contact density of a free Sn atom in several valence configurations. The contribution from the $[Kr]4d^{10}$ core is separated out as $\rho_{core}(0)$, whereas $\rho_{val}(0)$ is the contribution from the fifth shell. Units are a_0^{-3}.

Configuration	$\rho_{core}(0)$	$\rho_{val}(0)$
$5s^25p^2$	183 254.51	76.93
$5s^25p^1$	183 254.82	80.82
$5s^25p^0$	183 255.59	85.25
$5s^15p^3$	183 254.87	41.04
$5s^15p^2$	183 255.13	43.23
$5s^15p^1$	183 255.86	45.21
$5s^15p^0$	183 257.30	47.13
$5s^05p^4$	183 255.27	1.25
$5s^05p^3$	183 255.54	1.45
$5s^05p^2$	183 256.18	1.66
$5s^05p^1$	183 257.53	0.94
$5s^05p^0$	183 259.93	0.00

the volume dependence of the electron contact density. The results are listed in Table VII, which also quotes the β-Sn results for comparison. The calculated α-Sn equilibrium lattice constant is only 0.7% from the experimental value, whereas the β-Sn lattice constant is 4% too small. The bulk moduli are in very good agreement with experiments. (An earlier measurement of the bulk modulus of α-Sn of 1.2 Mbar (Ref. 80) appears to be at variance with both the measurement of Ref. 78 and the theoretical calculations of Refs. 28, 42, and 81, which get 709, 456, and 420 kbar, respectively, for this quantity.) The volume dependence of the electron contact density in β-Sn is 15% off the experimental value, which we consider an excellent result taking into consideration the relative scarce experimental information. Unfortunately, no data on the pressure variation of the electron contact density in α-Sn is available, which is mainly due to experimental difficulties, as the α phase readily transforms into the β phase upon pressure. We note, however, that it is of the same unusual sign[76] and the same magnitude as in β-Sn.

To test the validity of the frozen-core approximation in connection with calculations of the electron contact density, we list in Table VIII the results of some calculations (LDA, fully relativistic) of a free Sn atom in various charge states. The electron contact density is split up into the contribution from the $[Kr]4d^{10}$ core and the valence contribution. Except for the case of the fully ionized Sn^{4+} ion, the core contribution to the electron contact density varies a little, even when large fluctuations in valence configuration is imposed. As the actual variations in occupancy numbers of Table VI are less drastic, we do not feel uncomfortable about the frozen-core approximation. In fact, it is not difficult to build into the LMTO scheme a self-consistency procedure for the core, which is what is needed to perform a stringent test of the frozen-core approximation, but the values of Table VIII seem to suggest that the effort is not worthwhile, as the variation of electron contact density in solids primarily is an effect of the variation of the valence charge distribution with chemical composition.

V. CONCLUSION

In this work we have calculated the electronic structure of a series of crystals, in which Sn is found as a component. The band structures were discussed both in relation to experimental information and in relation to previous theoretical investigations. The electronic charge density on the site of the Sn nucleus was calculated and compared with experimental isomer shifts. The agreement was excellent, providing for the first time a truly parameter-free calibration of the ^{119}Sn isomeric transition with a 5% accuracy. The same result is a powerful test of the LMTO calculational scheme since it is applied to so different crystal structures and yet produces so good linearity of the isomer shift versus contact density curve. The decomposition of the crystal wave function into angular momentum character within each atomic sphere was demonstrated to be very convenient for interpreting the variations of the isomer shift with chemical environments.

ACKNOWLEDGMENTS

The authors are happy to express their warm gratitude to Dr. Hans L. Skriver, who supplied them with a copy of his LMTO codes.

*Present address: Max-Planck-Institut für Festkörperforschung, Heisenbergstrasse 1, D-7000 Stuttgart 80, Federal Republic of Germany.

[1]For a general review on Mössbauer spectroscopy, see *Mössbauer Isomer Shifts*, edited by G. K. Shenoy and F. E. Wagner (North-Holland, Amsterdam, 1978).
[2]P. A. Flinn, in *Mössbauer Isomer Shifts*, Ref. 1, Chap. 9a.
[3]G. Weyer, A. Nylandsted-Larsen, B. I. Deutch, J. U. Andersen,

and E. Antoncik, Hyperfine Interact. **1**, 93 (1975).
[4]G. Weyer, J. W. Petersen, S. Damgaard, H. L. Nielsen, and J. Heinemeier, Phys. Rev. Lett. **44**, 155 (1980); G. Weyer, J. W. Petersen, and S. Damgaard, in *Proceedings of the 12th International Conference on Defects in Semiconductors,* edited by C. A. J. Ammerlaan (North-Holland, Amsterdam, 1982).
[5]E. Antoncik, Hyperfine Interact. **11**, 265 (1981).
[6]E. Antoncik and B. L. Gu, in *Proceedings of the 12th International Conference on Defects in Semiconductors,* edited by C. A. J. Ammerlaan (North-Holland, Amsterdam, 1982).
[7]E. Antoncik and B. L. Gu, Hyperfine Interact. **14**, 257 (1983).
[8]O. H. Nielsen, F. K. Larsen, S. Damgaard, J. W. Petersen, and G. Weyer, Z. Phys. B **52**, 99 (1983).
[9]B. D. Dunlap and G. M. Kalvius, in *Mössbauer Isomer Shifts,* Ref. 1, Chap. 2.
[10]G. K. Shenoy and B. D. Dunlap, in *Mössbauer Isomer Shifts,* Ref. 1, Appendix IV.
[11]J. Speth, W. Henning, P. Kienle, and J. Meyer, in *Mössbauer Isomer Shifts,* Ref. 1, Chap. 13.
[12]F. Pleiter and H. de Waard, in *Mössbauer Isomer Shifts,* Ref. 1, Chap. 5c.
[13]H. Muramatsu, T. Minra, H. Nakahara, M. Fujoka, E. Tanaka, and A. Hashizume, Hyperfine Interact. **20**, 305 (1984).
[14]T. C. Tucker, L. D. Roberts, C. W. Nestor, T. A. Carlson, and F. B. Malik, Phys. Rev. **178**, 998 (1969).
[15]E. Antoncik, Phys. Rev. B **23**, 6524 (1981).
[16]E. Antoncik and B. L. Gu, Phys. Status Solidi B **111**, 261 (1982).
[17]O. K. Andersen, Phys. Rev. B **12**, 3060 (1975).
[18]H. L. Skriver, *The LMTO Method* (Springer, Berlin, 1984).
[19]P. Hohenberg and W. Kohn, Phys. Rev. **136**, B864 (1964); W. Kohn and L. J. Sham, Phys. Rev. A **140**, 1133 (1965).
[20]*Theory of the Inhomogeneous Electron Gas,* edited by S. Lundqvist and N. H. March (Plenum, New York, 1983).
[21]S. H. Vosko, L. Wilk, and M. Nusair, Can. J. Phys. **58**, 1200 (1980).
[22]In this work the radial Dirac equation is used, with the spin-orbit term omitted (the scalar-relativistic approximation), as described in Ref. 18, p. 219. The relatively high atomic number of Sn, $Z=50$, makes relativistic effects important in crystals containing tin. The neglect of spin-orbit coupling leads to inaccurate energy bands, but the self-consistent charge density is not expected to be very much influenced by this approximation. However, the scalar-relativistic effects are of significant importance, e.g., for the Sn electron contact density they lead to a factor 2.3 higher values than nonrelativistic calculations. It is therefore imperative to include scalar-relativistic effects in the calculations of properties related to Mössbauer isomer shifts. See Ref. 23 for a general discussion of relativistic effects.
[23]G. B. Bachelet and N. E. Christensen, Phys. Rev. B **31**, 879 (1985).
[24]J. Keller, J. Phys. C **4**, L85 (1971); D. Glötzel, B. Segall, and O. K. Andersen, Solid State Commun. **36**, 403 (1980).
[25]O. Jepsen and O. K. Andersen, Solid State Commun. **9**, 1763 (1971); G. Lehman and M. Taut, Phys. Status Solidi B **54**, 469 (1972).
[26]D. L. Price and J. M. Rowe, Solid State Commun. **7**, 1433 (1969); J. Thewlis and A. R. Davey, Nature (London) **174**, 1011 (1959).
[27]A. Svane (unpublished). This "naive" addition of the terms $\langle \chi_L \mid \Delta V \mid \chi_{L'} \rangle$ to the LMTO Hamiltonian matrix actually overestimates the effects of the nonspherical modulation of the crystal potential. This is due to the neglect of overlaps in the evaluation of the above matrix elements and to the fact that the combined correction term already has included a crude correction for the nonspherical potential in standard LMTO calculations. The self-consistent crystal charge density is not affected significantly but in α-Sn it has the qualitative effect of lifting the L_1 conduction state above the Γ'_{25} top valence state to produce a genuine semimetal, as it should be.
[28]G. P. Srivastava, J. Phys. C **16**, 1649 (1983).
[29]F. H. Pollak, M. Cardona, C. W. Higginbotham, F. Herman, and J. P. Van Dyke, Phys. Rev. B **2**, 352 (1970).
[30]S. Groves and W. Paul, Phys. Rev. Lett. **11**, 194 (1963).
[31]H. Höchst and I. Hernandez-Calderon, Surf. Sci. **126**, 25 (1983).
[32]M. L. Cohen and T. K. Bergstresser, Phys. Rev. **141**, B789 (1966).
[33]F. Herman, R. L. Kortum, C. D. Kuglin, and R. A. Short, in *Quantum Theory of Atoms, Molecules and the Solid State,* edited by P. O. Löwdin (Academic, New York, 1966).
[34]D. R. Hamann, Phys. Rev. Lett. **42**, 662 (1979).
[35]J. A. Rayne and B. S. Chandrasekhar, Phys. Rev. **120**, 1658 (1960).
[36]H. Olijnyk, S. K. Sikka, and W. B. Holzapfel, Phys. Lett. **103A**, 137 (1984).
[37]R. Biswas, R. M. Martin, R. J. Needs, and O. H. Nielsen, Phys. Rev. B **30**, 3210 (1984).
[38]M. Miasek and M. Suffczynski, Bull. Acad. Pol. Ser. Sci. Math. Astron. Phys. **9**, 477 (1961); **9**, 483 (1961); **9**, 489 (1961); M. Miasek, Phys. Rev. **130**, 11 (1963).
[39]G. Weisz, Phys. Rev. **149**, 504 (1966).
[40]J. E. Craven, Phys. Rev. **182**, 693 (1969).
[41]M. A. E. A. Ament and A. R. de Vroomen, J. Phys. F **4**, 1359 (1974).
[42]J. Ihm and M. L. Cohen, Phys. Rev. B **23**, 1576 (1981).
[43]P. M. Th. M. van Attekum and J. M. Trooster, J. Phys. F **9**, 2289 (1979).
[44]Estimates of the present authors on the basis of data published in Ref. 43.
[45]*Physics of IV-VI Compounds and Alloys,* edited by S. Rabii (Gordon and Breach, Oxford, 1974).
[46]L. Muldawer, Bull. Am. Phys. Soc. **16**, 84 (1971).
[47]V. Fano and I. Ortalli, J. Chem. Phys. **61**, 5017 (1974).
[48]V. G. Losev, S. S. Kabalkina, and L. F. Vereshchagin, Fiz. Tverd. Tela (Leningrad) **12**, 2942 (1970) [Sov. Phys.—Solid State **12**, 2374 (1971)].
[49]G. Lucovsky, R. M. Martin, and E. Burstein, in *Physics of IV-VI Compounds and Alloys,* Ref. 45, p. 93.
[50]*Table of Periodic Properties of the Elements* (Sargent-Wells Scientific, Chicago, 1968). For the ionic radius of Sn^{+3} we used the mean of those appropriate to Sn^{+2} and Sn^{+4}.
[51]R. W. G. Wyckoff, *Crystal Structures,* 2nd ed. (Wiley, New York, 1965), Vol. I.
[52]F. Herman, R. L. Kortum, I. B. Ortenburger, and J. P. Van Dyke, J. Phys. (Paris) **128**, 62 (1967).
[53]S. Rabii, Phys. Rev. **182**, 821 (1969).
[54]Y. W. Tung and M. L. Cohen, Phys. Rev. **180**, 823 (1969).
[55]R. L. Bernick and L. Kleinmann, Solid State Commun. **8**, 569 (1970).
[56]J. Robertson, Phys. Rev. B **28**, 4671 (1983).
[57]J. S. Melvin and D. C. Hendry, J. Phys. C **12**, 3003 (1979).
[58]K. M. Rabe and J. O. Joannopoulos, Phys. Rev. B **32**, 2302 (1985).
[59]A. Baldereschi, Phys. Rev. B **7**, 5212 (1973); D. J. Chadi and M. L. Cohen, *ibid.* **8**, 5747 (1973).
[60]P. C. Kemery and M. Cardona, J. Phys. C **9**, 1361 (1976).

[61]R. B. Shalvoy, G. B. Fischer, and P. J. Stiles, Phys. Rev. B **15**, 2021 (1977).
[62]Y. Ota and S. Rabii, in *Physics of IV-VI Compounds and Alloys,* Ref. 45, p. 113.
[63]Y. W. Tsang and M. L. Cohen, Phys. Rev. B **3**, 1254 (1971).
[64]F. Aymerich and G. Mula, Phys. Status Solidi B **42**, 697 (1970).
[65]M. Y. Au-Yang and M. L. Cohen, Phys. Rev. **178**, 1358 (1969).
[66]M. Cardona, J. Tejeda, N. J. Shevchik, and D. W. Langer, Phys. Status Solidi B **58**, 483 (1973).
[67]J. Tejeda, M. Cardona, N. J. Shevchik, D. W. Langer, and E. Schönherr, Phys. Status Solidi B **58**, 189 (1973).
[68]H. G. Lipson and A. Kahan, Phys. Rev. **133**, A800 (1964).
[69]See, e.g., Table I of N. E. Christensen and O. B. Christensen, Phys. Rev. B **33**, 4739 (1986).
[70]A. Svane and E. Antoncik, J. Phys. Chem. Solids (to be published).
[71]Experimental isomer shifts are taken from the 1983 Standard Reference Table [J. G. Stevens, Hyperfine Interact. **13**, 221 (1983)], except the value for SnSb, which is a weighted average of the shifts reported in Ref. 72.
[72]V. A. Bryukhanov, N. N. Delyagin, R. N. Kuzmin, and V. S. Shpinel, Zh. Eksp. Teor. Fiz. **46**, 1996 (1964) [Sov. Phys.—JETP **19**, 1344 (1964)]; H. Z. Dokuzoguz, L. H. Bowen, and H. H. Stadelmaier, J. Phys. Chem. Solids **31**, 1565 (1970). The isomer shift of this work was corrected by subtraction of 0.37 mm/sec from the reported value, in accordance with the improved calibration of the experimental equipment [H. Z. Dokuzoguz, H. H. Stadelmaier, and L. H. Bowen, J. Less-Common Mater. **23**, 245 (1971)]; V. T. Shupatov and P. P. Ceregin, Teor. Eksp. Khim. **8**, 413 (1972); F. Ambe and S. Ambe, J. Chem. Phys. **73**, 2029 (1980).
[73]A. Svane and E. Antoncik (unpublished).
[74]E. Antoncik, Hyperfine Interact. **11**, 265 (1981).
[75]R. M. Friedman, R. E. Watson, J. Hudis, and M. L. Perlman, Phys. Rev. B **8**, 3569 (1973).
[76]A. Svane and E. Antoncik, Solid State Commun. **58**, 541 (1986).
[77]D. G. Pettifor, Commun. Phys. **1**, 141 (1976).
[78]C. J. Buchenauer, M. Cardona, and F. H. Pollak, Phys. Rev. B **3**, 1243 (1971).
[79]In the range 0—100 kbar. Estimate of D. L. Williamson (in *Mössbauer Isomer Shifts,* Ref. 1, Chap. 6b).
[80]P. J. Reddy and S. V. Sabrahmanyan, Nature (London) **185**, 29 (1960).
[81]C. O. Rodriguez, V. A. Kuz, E. L. Peltzer y Blanca, and O. M. Cappanini, Phys. Rev. B **31**, 5327 (1985).